

The Change of Corrosion Inhibition Behavior of Tetradecyl Phosphate Ester at Elevated Temperatures

Shuai Ren, Yi He, Xi Wang, David Young, Marc Singer
Institute for Corrosion and Multiphase Technology
Department of Chemical and Biomolecular Engineering
Ohio University
342 West State Street
Athens, OH 45701, USA

Maalek Mohamed-Saïd
TotalEnergies
OneTech - CSTJF, Avenue Larribau
F-64018 Pau, France

Sheyla Camperos
TotalEnergies
OneTech - TRTG - TotalEnergies Research & Technology Gonfreville
BP 27 76 700 Harfleur, France

ABSTRACT

Having a better understanding of the effect of increased temperature on the performance of organic corrosion inhibitors (CIs) is beneficial for their usage in high temperature environments. The present work focuses on studying the effect of temperature on inhibition behaviours of an in-house synthesized CI model compound, tetradecyl phosphate ester (PE-C14), in a simulated refinery environment. Surface saturation concentrations at three temperatures (25°C, 55°C, and 80°C) are determined by exploiting corrosion rate evolution. At low temperature (25°C), a gelatinous film formed on the rotating cylinder electrode (RCE) surface that significantly affected the limiting current, although the PE-C14 layer was poorly adherent. At elevated temperatures (55°C and 80°C), a thick, adherent and readily detectable by EDS and Raman spectroscopy, PE-C14 layer formed on the RCE surface to achieve much lower corrosion rate (inhibition efficiency close to 100%) with relatable surface saturation concentrations.

Keywords: corrosion inhibition, phosphate ester, surface saturation concentration, temperature, inhibitor film

INTRODUCTION

Organic corrosion inhibitors (CIs) are widely employed in the oil and gas industry to protect carbon steel pipelines against internal corrosion. The high inhibition efficiency of organic CIs at extremely low concentration can be attributed to their amphiphilic molecular structures. This structure enables the formation of self-assembled films that act against corrosion *via* the adsorption of their hydrophilic head group on the steel substrate and the repulsion of aqueous corrosive species by their hydrophobic tail. Consequently, any factors affecting the film formation of organic CIs could lead to changes in inhibition behaviors.

The use of organic CIs in high-temperature environments, *i.e.*, up to 80°C here, has particular challenges: not only uninhibited corrosion rates (CRs) are largely accelerated, but also inhibition performance could be affected dramatically. The high temperature could affect the organic CIs inhibition performance from different aspects, such as influencing the adsorption process,¹⁻⁵ inducing chemical degradation,^{6, 7} enabling polymerization,^{8, 9} etc. Even through the performances of organic CIs at elevated temperatures have been extensively studied,¹⁻⁹ the mechanisms behind these effects require further elucidation. Moreover, the effects of temperature on inhibition are often different from inhibitor to inhibitor. Consequently, more research work about the effect of high temperature on organic CIs will be beneficial for their optimal usage.

The research described herein focuses on studying the effect of temperature on inhibition behaviours of an in-house synthesized CI model compound, tetradecyl phosphate ester (PE-C14), in a simulated refinery environment. Surface saturation concentrations at three temperatures are identified in relation to corrosion rate over time measurements obtained by linear polarization resistance (LPR). Potentiodynamic sweeps were collected after the corrosion rate stabilized. Surface analysis techniques, including scanning electron microscopy (SEM), energy dispersive X-ray spectroscopy (EDS), and Raman spectroscopy, were employed to characterize the specimen surfaces after their exposure to the experimental environment at the selected temperatures. This paper mainly focuses on describing experimental observations and raising relevant research questions, mechanistic interpretation is ongoing and will be the subject of a future publication.

EXPERIMENTAL SETUP AND METHODOLOGY

Materials and Chemicals

Steel specimens used for electrochemical measurements were machined from UNS G10180* carbon steel (C1018) with a ferritic-pearlitic microstructure. The in-house synthesized CI model compound, tetradecyl phosphate ester (PE-C14), was employed in this work. The composition of PE-C14 consists of 73.5% monoester and 26.5% diester. Their molecular structures are shown in Figure 1. Its synthesis, purification, and characterization are described elsewhere.¹⁰

* UNS numbers are listed in *Metals and Alloys in the Unified Numbering System*, published by the Society of Automotive Engineers (SAE International) and cosponsored by ASTM International.



Figure 1: Molecular structures of in-house synthesized tetradecyl phosphate ester (PE-C14) (monoester and diester present as 3:1 mixture)

Apparatus and Electrochemical Techniques

The electrochemical measurements were carried out using a three-electrode glass cell (Figure 2) with a platinum grid as a counter electrode, saturated KCl Ag/AgCl reference electrode, and a C1018 rotating cylinder electrode (RCE) with an outer diameter of 12 mm and a height of 14 mm as a working electrode. All potentials reported in this paper are in reference to a saturated KCl Ag/AgCl electrode. The reference electrode was connected to the corrosion cell *via* a KCl salt bridge and a Luggin capillary.

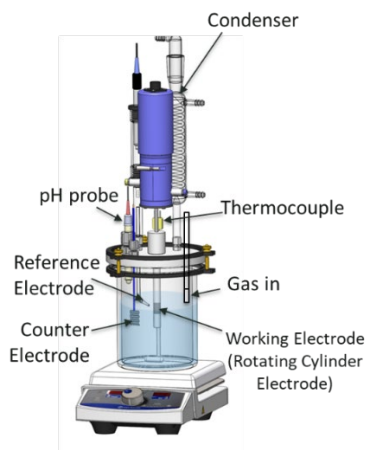


Figure 2: Schematic of the setup for electrochemical experiments[†]

Corrosion rate was assessed by linear polarization resistance (LPR) measurements, with a scan range from -5 mV to +5 mV vs. OCP, a scan rate of 0.125 mV/s and a B value of 26 mV. Cathodic potentiodynamic polarization sweeps were conducted at the end of each experiment when the corrosion rates were stable, by starting from the OCP down to -0.6 V vs. OCP at a scan rate of 0.125 mV/s. The anodic potentiodynamic sweeps were taken subsequently when the OCP returned to the original value before the cathodic sweep; they were taken from the OCP up to +0.2 V vs. OCP. The ohmic drop was compensated for in all the presented curves. All electrochemical measurements were carried out *via* a potentiostat (Gamry Interface 1010[‡]). The error bars shown on the curves throughout this paper indicate the minimum and maximum values from multiple measurements.

[†] Image courtesy of Cody Shafer, ICMT, Ohio University.

[‡] Trade name

© 2022 Association for Materials Protection and Performance (AMPP). All rights reserved. No part of this publication may be reproduced, stored in a retrieval system, or transmitted, in any form or by any means (electronic, mechanical, photocopying, recording, or otherwise) without the prior written permission of AMPP.

Positions and opinions advanced in this work are those of the author(s) and not necessarily those of AMPP. Responsibility for the content of the work lies solely with the author(s).

Test Matrix and Procedure

The corrosion experiments were performed in a simulated refinery environment containing low NaCl concentration (0.1 wt.%) with NH₄OH (ammonium hydroxide) and CH₃COOH (acetic acid) as other aqueous components. The full experimental matrix is shown in Table 1. A schematic of the experimental procedure is shown in Figure 3. Prior to each experiment, the RCE was sequentially polished with 180, 400 and 600 grit silicon carbide abrasive papers, cleaned with isopropanol in an ultrasonic bath after polishing, and air-dried before insertion into the cell. The solution was deoxygenated for 2 hours by sparging with N₂ prior to the introduction of the working electrode. Before the injection of PE-C14, there was 20 minutes of pre-corrosion, in which LPR, OCP and EIS measurements were taken to ensure that there was no contamination from previous experiments and the surface conditions of the steel specimens were consistent among all sets of tests. After the injection of Cls, LPR and EIS data were taken every 30 minutes until the corrosion rate became stable (± 0.01 mm/year). At the end of each test, potentiodynamic polarizations were conducted. The N₂ saturated solution was maintained at pH 3.8 by injecting NaOH and HCl solutions. Sparging with N₂ was maintained throughout the test to prevent air ingress and maintain the saturation of the test electrolyte with N₂. The rotation speed of the working RCE was set at 1000 rpm before starting the electrochemical measurements. The PE-C14 inhibitor model compound was dissolved in isopropyl alcohol first and then this mixture was deoxygenated with N₂ and injected into solution directly using a long syringe needle.

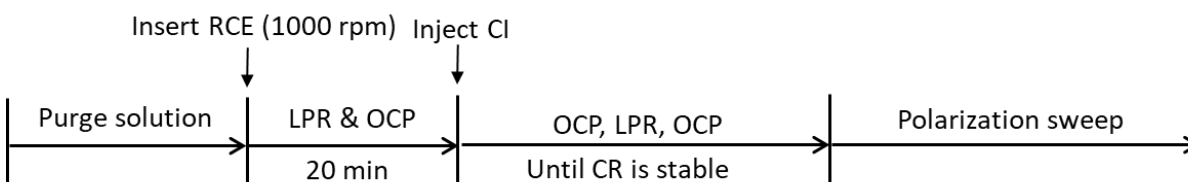


Figure 3: General experimental procedure for electrochemical experiments

Table 1. Experimental matrix for electrochemical experiments

Description	Parameters
Working solution	0.1 wt.% NaCl, 30 mg/L HCl 37%, 10 mg/L NH ₄ OH, 50 mg/L HAc
Material	UNS G10180
Sparge gas	N ₂
Total pressure	1 bar
Temperature	25°C, 55°C and 80°C
pH	3.8 \pm 0.1
Cl model compound	PE-C14

Other analytical techniques were also used for post-exposure analysis. Raman spectroscopy was conducted to capture the Raman peaks of surface products using 532 nm laser with 2.5 mW and 3 s dwell time. Scanning electron microscopy (SEM) and energy dispersive spectroscopy (EDS) were also used to capture secondary electron images and elemental information. The secondary electron images were taken with an accelerating voltage of 15 kV, and spot size of 60.

EXPERIMENTAL RESULTS AND DISCUSSION

Determination of Surface Saturation Concentration

As described by Hackerman, *et al.*,¹¹ the surface saturation concentration is the critical bulk Cl concentration for which the metal surface is assumed to be saturated with the adsorbed inhibitor molecules, resulting in minimal corrosion rate and maximal inhibition efficiency. It can be determined by comparing the stable corrosion rates of metal specimens exposed to different Cl concentrations.

Results of corrosion rate evolution with time for C1018 in the studied environment over a range of PE-C14 concentrations at 25°C, 55°C and 80°C are shown in Figure 4. At 25°C (Figure 4a), in blank condition, the corrosion rate decreased at the initial stage and then stabilized between 0.5 to 1.0 mm/year. The stable corrosion rates decreased with the addition of PE-C14 concentration but only until a Cl concentration of 40 ppm_w was reached. However, when the PE-C14 concentration surpassed 40 ppm_w, the corrosion rate of C1018 did not decrease further and stabilized at ca. 0.06 to 0.02 mm/year. Therefore, the critical concentration for PE-C14 to achieve surface saturation in the studied environment at 25°C

The surface saturation concentrations of PE-C14 at 55°C and 80°C were determined following the same method. At 55°C (Figure 4b), the corrosion rate stabilized between 3 to 4 mm/year in the blank test. In inhibited tests, the surface saturation is achieved between 40 and 60 ppm_w with a stabilized inhibited corrosion rate at ca. 0.002 mm/year. This implies that the time taken to completely corrode a 1cm thick piece of the tested steel would be increased from 3 years to 5000 years in the presence of PE-C14 at this critical concentration. At 80°C (Figure 4c), a similar stabilized corrosion rate ca. 0.002 mm/year was achieved by a higher surface saturation concentration between 80 and 160 ppm_w. As a comparison, the uninhibited “blank” corrosion rate was between 7.5 to 11 mm/year.

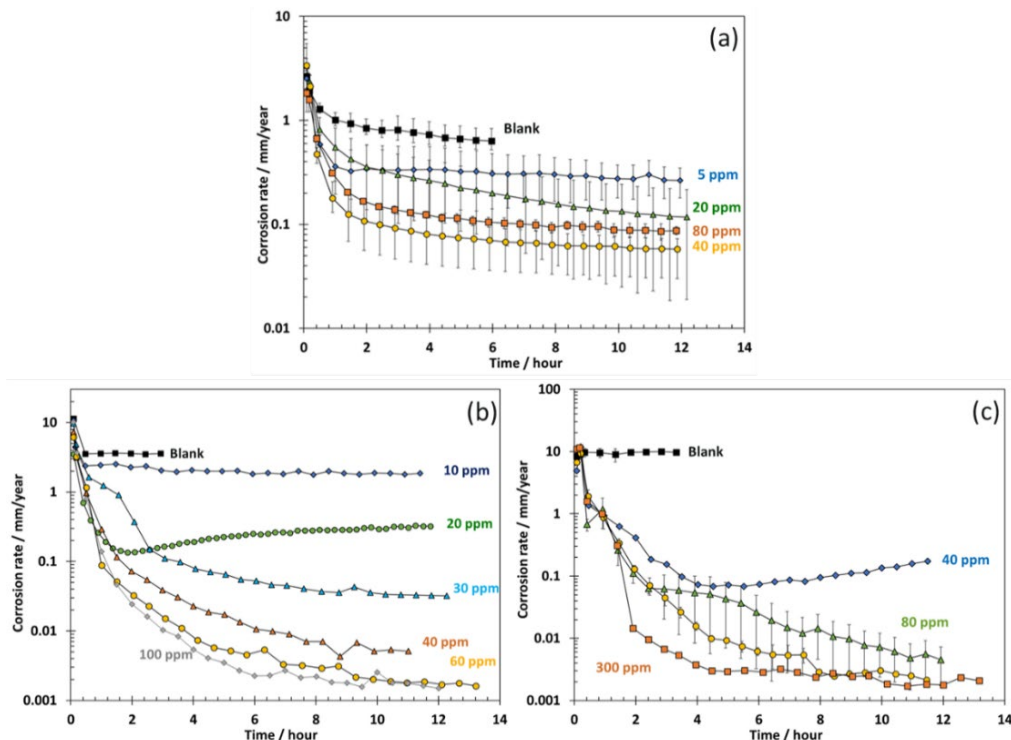


Figure 4. Corrosion rate vs. time of C1018 in simulated refinery environment with different PE-C14 concentrations at 25°C (a), 55°C (b) and 80°C (c).

© 2022 Association for Materials Protection and Performance (AMPP). All rights reserved. No part of this publication may be reproduced, stored in a retrieval system, or transmitted, in any form or by any means (electronic, mechanical, photocopying, recording, or otherwise) without the prior written permission of AMPP.

Positions and opinions advanced in this work are those of the author(s) and not necessarily those of AMPP. Responsibility for the content of the work lies solely with the author(s).

Potentiodynamic polarization curves of C1018 in the studied environment with different PE-C14 concentrations at 25°C, 55°C and 80°C are shown in Figure 5. Comparing the experiments containing PE-C14 with the blank test, it can be seen that both anodic and cathodic polarization curves were retarded. This inhibition behavior was consistent among all three studied temperatures. At 25°C (Figure 5a), as the concentration reached above 40 ppm_w, the charge transfer of both the anodic and cathodic regions show no more retardation. It is confirmed that the surface saturation concentration was between 20 and 40 ppm_w in the studied conditions. Similarly, the surface saturation concentrations determined from corrosion rate results can be confirmed by the polarization curves at 55°C.

The limiting current density was affected by one order of magnitude in the inhibited experiments at 25°C, as shown in Figure 5a. As temperature increased to 55°C (Figure 5b), the limiting currents slightly decreased in inhibited cases. However, significant effects on limiting currents were observed again under inhibited conditions at 80°C, as displayed by Figure 5c. More discussion about the limiting current change is made in a later section.

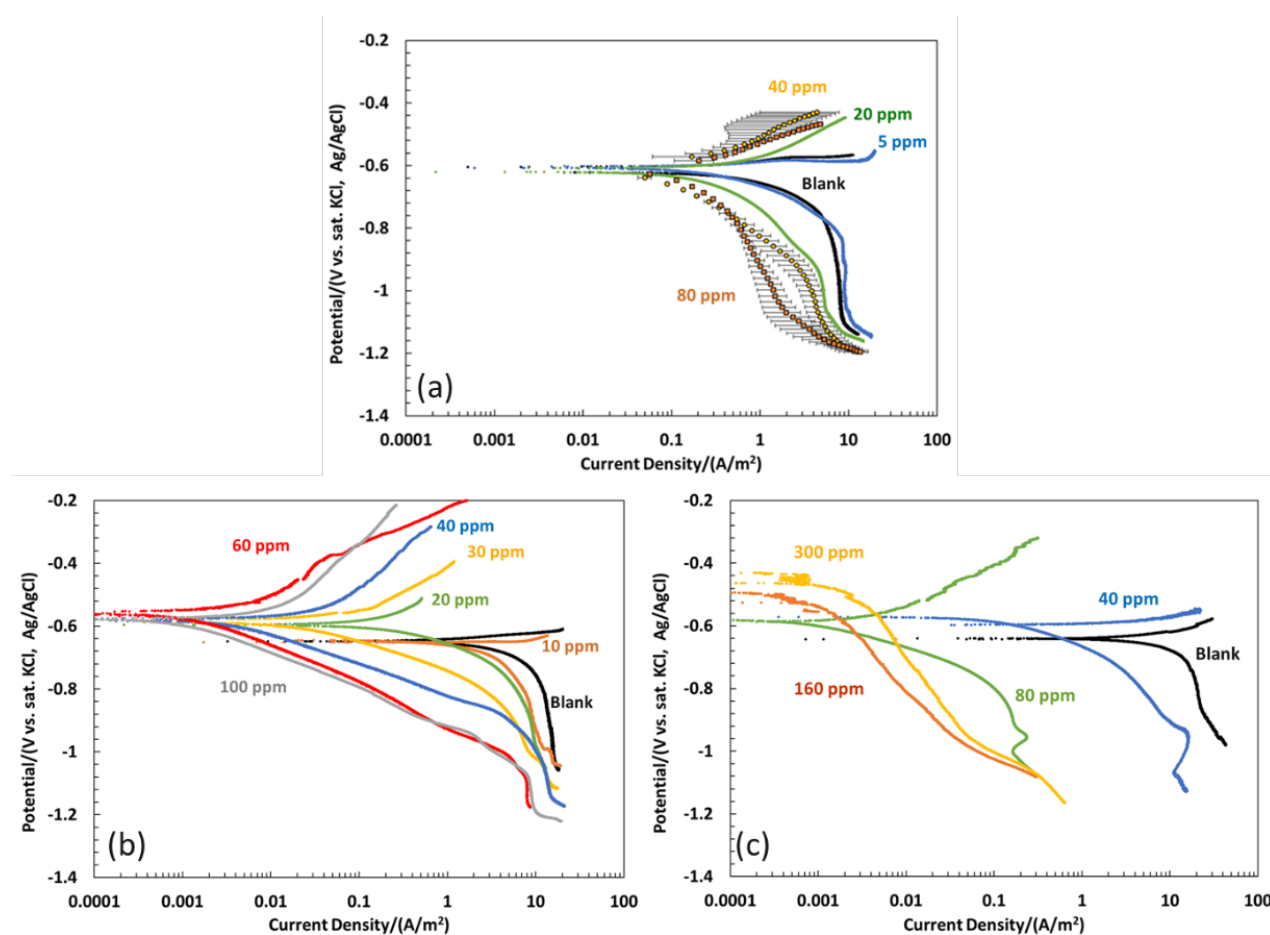


Figure 5. Potentiodynamic polarization curves of C1018 in simulated refinery environment with different PE-C14 concentrations at 25°C (a), 55°C (b) and 80°C (c).

The inhibition performance at different temperatures in the studied environment are compared in Table 2 to understand the effect of temperature on inhibition of PE-C14. The surface saturation concentrations increased as temperature increased. The baseline corrosion rate increased with temperature since this accelerates both the anodic and cathodic reactions, thus promoting corrosion. Higher baseline corrosion

rate requires higher PE-C14 concentration to mitigate corrosion to the minimum corrosion rate, thus, higher surface saturation concentration is required. As for the stable corrosion rates at surface saturation concentrations, the corrosion rates at 55°C and 80°C (ca. 0.002 mm/year) were much lower than that at 25°C (ca. 0.06 to 0.02 mm/year). Consequently, the inhibition efficiencies (IEs) at surface saturation concentration at 55°C and 80°C (~ 100%) were higher than the IE at 25°C (93% ± 5%). These changes over temperature are discussed in depth with corresponding surface analysis results in the next section.

Table 2. Comparison of inhibition performances of PE-C14 at different temperatures in simulated refinery environment.

Temperature (°C)	Surface saturation concentration (SSC) (ppm _w)	Baseline CR (mm/yr)	Stable CR at SSC (mm/yr)	IE at SSC
25	20 to 40	0.5 to 1	0.06 to 0.02	93% ± 5%
55	40 to 60	3 to 4	~ 0.002	~ 100%
80	80 to 160	7.5 to 11	~ 0.002	~ 100%

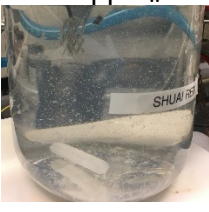
Experimental Observation and Surface Analysis

Besides inhibition performance, the RCE specimen surfaces and solutions during and after the experiments also showed some differences at different temperatures. Table 3 summarizes these differences, including RCE surface morphology and solution appearance after electrochemical experiments.

At 25°C, a gelatinous film on the RCE specimen surface was observed, as displayed by the images in Table 3. This gelatinous film could be washed off easily and the steel surface exposed when rinsed by deionized water and isopropyl alcohol. At the end of the experiments, the solution had become cloudy, and agglomerates were observed floating on and suspending in the experimental solutions, as shown in Table 4.

At 55°C, a visible whitish layer was formed on the RCE specimen surface, as shown by the picture in Table 3. Different from the gelatinous film formed at 25°C, the whitish layer still adhered to the surface after being rinsed by deionized water and isopropyl alcohol. As for the electrolyte appearance, it became cloudy immediately as the PE-C14 was injected therein. As the experiment proceeded, the test electrolyte gradually became clearer, but with aggregated PE-C14 molecules colloiddally suspended in the solution. At 80°C, the RCE specimen morphology and solution appearance were essentially the same as those observed at 55°C.

Table 3. Comparison of RCE specimen surface morphology and solution appearance after the electrochemical experiments at different temperatures in simulated refinery environment.

T (°C)	RCE morphology after electrochemical experiments		Electrolyte appearance after electrochemical experiments	
	40 ppm _w	80 ppm _w	40 ppm _w	80 ppm _w
25				
55			Cloudy, aggregated compounds floated on and suspended in the solution (similar to the appearance at 25°C with 40 ppm _w PE-C14)	
80	Visible whitish layer (similar to the layer formed at 55°C)		Cloudy, aggregated compounds floated on and suspended in the solution (similar to the appearance at 25°C with 40 ppm _w PE-C14)	

Raman spectroscopy and SEM/EDS techniques were then used to have a better understanding about the layers formed on RCE specimen surfaces at different temperatures. The RCE specimens were rinsed by deionized water and isopropyl alcohol, sequentially, and then dried by compressed air before the Raman spectroscopy. The Raman spectra of RCE specimen surfaces after electrochemical experiments at 25°C and 80°C with 40 ppm_w PE-C14 are shown in Figure 6. The pure solid PE-C14 was measured first and its peaks were detected, as shown in Figure 6. Identical peaks were detected on the RCE specimen retrieved from the condition at 80°C with 40 ppm_w PE-C14. However, no PE-C14 peaks was shown on the RCE specimen extracted from the condition at 25°C with 40 ppm_w PE-C14 after rinsing.

The composition of the whitish layer formed on the RCE surfaces at both 55°C and 80°C needed to be determined - whether it was corrosion product, intact, or decomposed corrosion inhibitor. This layer was then reproduced on a flat specimen surface and characterized using SEM and EDS. The flat specimen was immersed in the studied environment at 80°C with 300 ppm_w PE-C14 for 12 hours and then extracted for surface analysis. The cross-section SEM image and EDS mapping results are shown in Figure 7. The SEM image clearly shows a layer, around 30 to 60 μm in thickness, present on the steel surface. The layer was phosphorus-rich according to EDS mapping. The EDS result confirmed that this layer was composed of PE-C14.

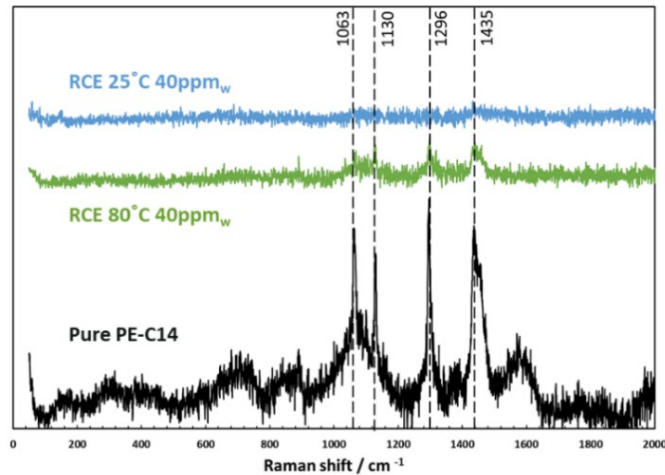


Figure 6. The Raman spectroscopy results detected on RCE specimen surfaces after electrochemical experiments at 25°C and 80°C in simulated refinery environment in the presence of 40 ppm_w PE-C14.

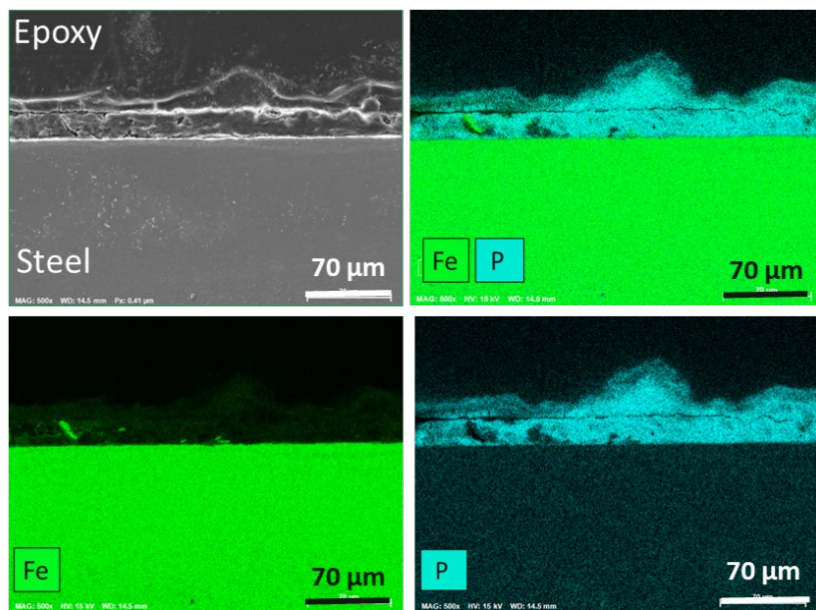


Figure 7. Cross-section SEM image (top-left) and EDS mapping results of flat specimen after 12 hours immersion in simulated refinery environment at 80°C in the presence of 300 ppm_w PE-C14.

Discussion

Both electrochemical and surface analysis results showed some differences between low temperature (25°C) and high temperatures (55°C and 80°C) inhibition experiments. The potential connections between the electrochemical and surface analysis results at different temperatures indicate the following. At low temperature (25°C), a gelatinous film was formed on the RCE surface, which could be rinsed off easily by deionized water and isopropyl alcohol. No PE-C14 was detected on RCE specimen surface (with gelatinous film rinsed off) retrieved from the condition at 25°C with 40 ppm_w PE-C14. It can be hypothesized that a monolayer formed on the RCE surface, which was of nanometer scale and beyond

the detection limit of Raman spectroscopy. From the potentiodynamic polarization curves (Figure 5), the limiting current densities with 40 and 80 ppm_w of PE-C14 were distinctly retarded. It can be unequivocally stated that the gelatinous film on the RCE surface plays a role in impeding the mass transfer of hydrogen ions to the steel substrate. Consequently, the limiting current density diminished.

At elevated temperatures (55°C and 80°C), a visible whitish layer was formed on the RCE surface after the experiment, which was more adherent than the gelatinous film formed at 25°C. Intense PE-C14 signature peaks were detected by Raman spectroscopy on the RCE specimen surface after the experiment at 80°C with 40 ppm_w PE-C14, which implies the whitish layer is composed of intact PE-C14 molecules. A 30 to 60 μm phosphorus-riched layer from EDS mapping confirmed the formation of thick and dense PE-C14 layers at these higher temperatures. Consequently, it can be readily postulated that the whitish PE-C14 layer should be multilayer rather than monolayer. From the potentiodynamic polarization curves (Figure 5), the limiting current was retarded in inhibited conditions, which could be because this thick PE-C14 layer blocked active sites or acted as a mass transfer barrier for hydrogen ions. Besides, the stable CRs at surface saturation concentrations at 55°C and 80°C (ca. 0.002 mm/year) are much lower than that at 25°C (ca. 0.06 to 0.02 mm/year) (thus higher IEs at 55°C and 80°C), which could be due to the presence of this thick and adherent PE-C14 layer as well. It is noteworthy that no decomposition of the PE-C14 was observed.

The cloudiness after PE-C14 was injected into solutions can be related to its low solubility in water, especially at high temperatures. Many studies¹²⁻¹⁵ have reported the “cloud point” of nonionic surfactants in aqueous solutions. The solubility of nonionic surfactants in water mainly result from the formation of hydrogen bonding with water molecules¹². As temperature increases, hydrogen bonds break, thus, the surfactant solubility decreases. At a certain temperature, known as the “cloud point”, the surfactant molecules separate out of solution and cloudiness develops.^{12, 13} As a nonionic surfactant in acidic solution, the solubility of PE-C14 decreases as temperature increases. From the experimental observation, the “cloud point” of PE-C14 used in the current work should be lower than 55°C, since the cloudiness occurs at 55°C even with a very low concentration. At 25°C, the cloudiness tends to occur with high PE-C14 concentrations, due to exceeding the solubility of PE-C14. Even though the cloudiness occurs at three different temperatures, the layers formed on RCE specimen surfaces during experiments were totally different between low temperature (25°C) and the studied elevated temperatures (55°C and 80°C). This implies that the temperature affected the PE-C14 inhibition performance likely through playing a role in adsorption processes and layer formation, which will not be further discussed here. The mechanism behind the temperature effects is the subject of ongoing work.

CONCLUSIONS

Temperature plays a significant role in layer formation for an in-house synthesized tetradecyl phosphate ester (PE-C14) in the studied simulated refinery environment. Consequently, PE-C14 presented different inhibition performances at different temperatures. At low temperature (25°C), a gelatinous film formed on the RCE surface could affect the limiting current and the poorly adherent PE-C14 is undetectable on the RCE surface after rinsing. At higher temperatures (55°C and 80°C), a thick and adherent PE-C14 layer can form on the RCE surface to achieve much lower corrosion rates (higher inhibition efficiency) with surface saturation concentrations. The reason behind the effect of temperature on PE-C14 layer formation is currently under investigation.

ACKNOWLEDGEMENTS

This project has been supported by TotalEnergies transversal R&D project (MANA Project). The authors would like to thank TotalEnergies for their financial support and valuable discussions.

REFERENCES

- [1] P. Lowmunkhong, D. Ungthararak, and P. Sutthivaiyakit, "Tryptamine as a corrosion inhibitor of mild steel in hydrochloric acid solution," *Corros. Sci.*, vol. 52, no. 1, pp. 30–36, Jan. 2010, doi: 10.1016/j.corsci.2009.08.039.
- [2] F. Bentiss, M. Lebrini, and M. Lagrenée, "Thermodynamic characterization of metal dissolution and inhibitor adsorption processes in mild steel/2,5-bis(n-thienyl)-1,3,4-thiadiazoles/hydrochloric acid system," *Corros. Sci.*, vol. 47, no. 12, pp. 2915–2931, Dec. 2005, doi: 10.1016/j.corsci.2005.05.034.
- [3] X. Li, S. Deng, G. Mu, H. Fu, and F. Yang, "Inhibition effect of nonionic surfactant on the corrosion of cold rolled steel in hydrochloric acid," *Corros. Sci.*, vol. 50, no. 2, pp. 420–430, Feb. 2008, doi: 10.1016/j.corsci.2007.08.014.
- [4] G. Moretti, G. Quartarone, A. Tassan, and A. Zingales, "Inhibition of mild steel corrosion in 1N sulphuric acid through indole," *Mater. Corros.*, vol. 45, no. 12, pp. 641–647, Dec. 1994, doi: 10.1002/maco.19940451203.
- [5] E. E. Oguzie, "Evaluation of the inhibitive effect of some plant extracts on the acid corrosion of mild steel," *Corros. Sci.*, vol. 50, no. 11, pp. 2993–2998, Nov. 2008, doi: 10.1016/j.corsci.2008.08.004.
- [6] L. Zheng, J. Landon, N. C. Koebecke, P. Chandan, and K. Liu, "Suitability and Stability of 2-Mercaptobenzimidazole as a Corrosion Inhibitor in a Post-Combustion CO₂ Capture System," *Corrosion*, vol. 71, no. 6, pp. 692–702, Jun. 2015, doi: 10.5006/1524.
- [7] R. Solmaz, G. Kardaş, M. Çulha, B. Yazıcı, and M. Erbil, "Investigation of adsorption and inhibitive effect of 2-mercaptothiazoline on corrosion of mild steel in hydrochloric acid media," *Electrochim. Acta*, vol. 53, no. 20, pp. 5941–5952, Aug. 2008, doi: 10.1016/j.electacta.2008.03.055.
- [8] R. J. Tedeschi, "Acetylenic Corrosion Inhibitors," *Corrosion*, vol. 31, no. 4, pp. 130–134, Apr. 1975, doi: 10.5006/0010-9312-31.4.130.
- [9] G. W. Poling, "Infrared Studies of Protective Films Formed by Acetylenic Corrosion Inhibitors," *J. Electrochem. Soc.*, vol. 114, no. 12, p. 1209, 1967, doi: 10.1149/1.2426451.
- [10] Y. He, S. Ren, Z. Belarbi, X. Wang, D. Young, and M. Singer, "Micellization and Inhibition Efficiency," in *AMPP Int. Corros. Conf., 2021, paper no. 16872*.
- [11] T. Murakawa, S. Nagaura, and N. Hackerman, "Coverage of iron surface by organic compounds and anions in acid solutions," *Corros. Sci.*, vol. 7, no. 2, pp. 79–89, Jan. 1967, doi: 10.1016/S0010-938X(67)80105-7.
- [12] W. N. Maclay, "Factors affecting the solubility of nonionic emulsifiers," *J. Colloid Sci.*, vol. 11, no. 3, pp. 272–285, Jun. 1956, doi: 10.1016/0095-8522(56)90052-6.
- [13] A. M. Al-Ghamdi and H. A. Nasr-El-Din, "Effect of oilfield chemicals on the cloud point of nonionic surfactants," *Colloids Surfaces A Physicochem. Eng. Asp.*, vol. 125, no. 1, pp. 5–18, May 1997,

doi: 10.1016/S0927-7757(96)03860-5.

- [14] K. S. Sharma, S. R. Patil, and A. K. Rakshit, "Study of the cloud point of C12En nonionic surfactants: effect of additives," *Colloids Surfaces A Physicochem. Eng. Asp.*, vol. 219, no. 1–3, pp. 67–74, Jun. 2003, doi: 10.1016/S0927-7757(03)00012-8.
- [15] P. D. T. Huibers, D. O. Shah, and A. R. Katritzky, "Predicting Surfactant Cloud Point from Molecular Structure," *J. Colloid Interface Sci.*, vol. 193, no. 1, pp. 132–136, Sep. 1997, doi: 10.1006/jcis.1997.5053.